INTERNATIONAL JOURNAL OF OPTIMIZATION IN CIVIL ENGINEERING
Int. J. Optim. Civil Eng., 2019; 9(3):457-482

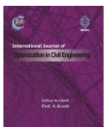

TOPOLOGY OPTIMIZATION OF PERFORATED STEEL PLATE SHEAR WALLS WITH THICK PLATE IN SIMPLE FRAMES

M.H. Bagherinejad and A. Haghollahi[*, †]
Faculty of Civil Engineering, Shahid Rajaee Teacher Training University, Tehran, Iran

ABSTRACT

In this paper, topology optimization (TO) is applied to determine the form, size and location of holes for the special form of perforated steel plate shear wall (PSPSW). The proposed model is based on the recently presented particular form of PSPSW that is called the ring-shaped steel plate shear wall. The strain energy is selected as the objective function in the optimization. Simple Isotropic Material with Penalization (SIMP) method and the solution algorithms, including sensitivity and condition-based methods are utilized in the TO. Four initial plate forms are presented in the TO with regards to the length of the connection between the plate and column. Based on the solution methods and initial forms of the plate, eight scenarios are proposed and seven different perforated plates obtained using TO. The nonlinear responses of the optimized perforated plates are compared together, and with the ring-shaped model as a benchmark. The nonlinear analysis is conducted under cyclic and monotonic loadings. Key issues include cyclic and monotonic behavior, pinching behavior, stiffness, load-carrying capacity, energy dissipation, fracture tendency and out-of-plane deformation are investigated and discussed. The results demonstrate the optimized models have better behavior than the ring-shaped model without changing the volume of the plate.

Keywords: topology optimization; perforated steel plate shear walls; SIMP method; sensitivity - based method; condition - based method.

Received: 18 October 2018; Accepted: 25 February 2019

1. INTRODUCTION

Steel plate shear wall (SPSW) is considered as an efficient lateral system in the seismic zones and tall buildings because of its special ability in the energy dissipation, ductility and

[*]Corresponding author: Faculty of Civil Engineering, Shahid Rajaee Teacher Training University, Tehran, Iran
[†]E-mail address: haghollahi@sru.ac.ir (A. Haghollahi)

resistance degradation under cyclic loading. The shear plate of SPSW generates the horizontal shear resistance in a story using tension field action. Ductility and energy dissipation are mainly achieved through yielding of the web plate along the tension field direction. The axial forces due to tension field have a considerable impact on the seismic behavior of the edge columns [1]. Another feature of SPSW is the significant development of the post-buckling shear capacity that causes tension field action to be created. On the other hand, the buckling and out-of-plane deformation (OPD) of SPSW due to lateral forces lead to a decrease in the stiffness and create the pinching behavior [2].

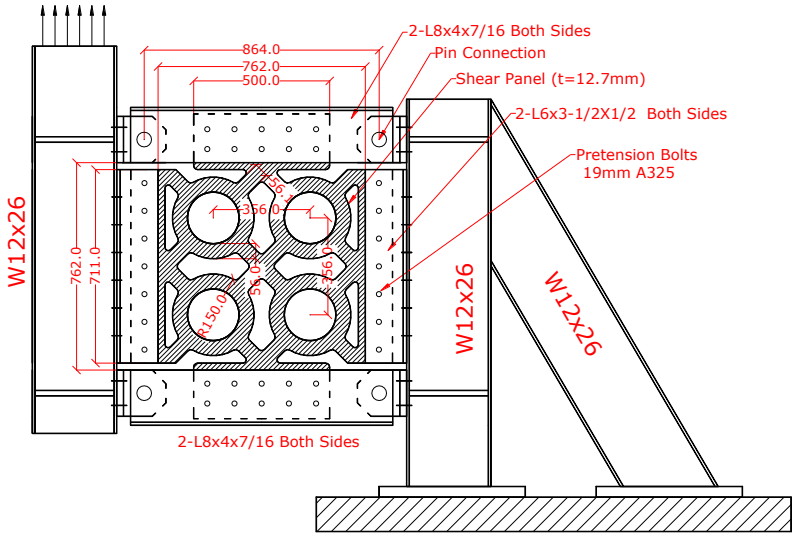

Figure 1. Ring-shaped model (Specimen 2-13-1)

There are two general approaches to improve the seismic performance of an SPSW. The first one is to enhance the out-of-plane stiffness of the plate and the second one is to provide a weak wall in front of a strong frame. Several studies have been carried out to increase the out-of-plane stiffness by making additional elements or new configuration of the SPSW. Using trapezoidal corrugated steel webs [3, 4], concrete panel on both sides of SPSW [5], vertical and horizontal plate stiffeners [6], additional diagonal elements [7] and braced steel shear panels [8] are the recent studies about the improvement of out-of-plane stiffness. Several researches have been conducted in the “strong frame-weak wall” field. For example, making a hole in the center of the plate or several holes in the plate [9], shear panel with vertical slits [10], steel plate shear wall with the low yield point material [11]. Wang, Yang [12] gave a comparative study on the seismic behavior of the SPSWs. The conducted studies indicate determining a suitable dimension and location for the holes has a considerable impact on the dynamic behavior of perforated steel plate shear wall (PSPSW). Egorova, Eatherton [13] introduced a special configuration of PSPSW that is called the ring-shaped steel plate shear wall. They improved the ductility, energy dissipation capacity and pinching behavior in cyclic loading through the mechanism of deforming a circular ring into an ellipse (see Fig. 1). Preparing the ring-shaped SPSW is very difficult in view of the cutting process and consequently increases the construction costs. But its behavior presents a new performance of SPSW in the simple frames.

By considering the forms of PSPSWs and conducted studies, probably the most important question is “which form of the PSPSW is the best form, and how could it be achieved”. Topology optimization (TO) could be the best tool to find the optimal form of the perforated plates. TO is a mathematical method to optimize the performance of the structures based on an objective function and constraints. TO determines the best form of material configuration within a given design space, set of loads, boundary conditions and constraints. TO of solid structures involves the specification of features such as the number, location and shape of holes and connectivity [14]. Bendsøe and Kikuchi [15] introduced the first topological optimization that was named generalized layout optimization method. Their method was applied to an elastic and two-dimensional stress problem. Gradually, much progress was made in TO. Introducing different solution methods, TO of structures considering the nonlinear behavior of material [16] and geometry [17], using different elements such as shell elements [18], TO of structures with regards to buckling phenomenon [19] and the effects of dynamic loads in TO [20] are some of the improvements that are related to the object of this study. The conducted developments have led to the application of TO in the complex problems. Professional programs such as TOSCA structure, Altair Hypermesh and Genesis have also been released. They are frequently updated based on the latest advancements in TO.

By taking a glance at the literature of TO, it is evident most of the conducted studies have been presented with the simple problems to illustrate their merits. It can be said one of the main purposes of the TO development is their use in the industrial and building structures in order to improve their performance and decrease their structural weight. So far, various studies have been done on the use of TO in industrial and building structures such as: topology of truss members [21-23], TO of concrete arch dams [24-26], TO of doms [27-29], masonry units with regard to heat loss [30], a side frame used in a railway freight wagon [31], GFRP bridge deck [32], braced frames under wind load using continuum, beam and column elements [33], bridge girder [34], continuum structures under buckling constraints [35], planar frames under seismic loads [36] and CFRP composites to retrofit beam-column connection [37].

Recently, a number of papers have been presented that used professional programs for TO of structures, such as: TO of roller bearing housing in order to maximize the bearing fatigue life using ANSYS and TOSCA [38], TO of vibro-acoustic hearing instrument based on minimization of the feedback signal and reduction of the time consumption using ABAQUS and TOSCA [39], TO of steel perforated I-sections in order to replace the traditional cellular beams using ANSYS and Altair Hypermesh [40], TO of a 12000KN fine blanking press using Altair Hypermesh [41] and TO of the photovoltaic panel connector in high-rise buildings using Altair Hypermesh [42] (see Fig. 2).

In this study, size, shape and location of the holes are determined using TO in PSPSW. In the second section, the ring-shaped steel plate shear wall [13] is modeled in ABAQUS using a shell element, and the cyclic behavior of the numerical model is compared with the experimental specimen. In the third section, TO is applied to the model using TOSCA [43] that is combined with ABAQUS [44]. The objective function, constraints, stop conditions and solution methods are defined for TO procedure. The effects of the sensitivity and condition-based methods and initial plate forms are investigated on the TO procedure and its results. Seven different forms of PSPSW are obtained using TO. In the fourth section, the nonlinear responses of the seven optimized forms are compared under cyclic and monotonic

loadings. In this section, the structural properties including stiffness, load-carrying capacity, pinching behavior, energy dissipation, fracture tendency and OPD of the optimized perforated plates are discussed in detail and compared to the ring-shaped model.

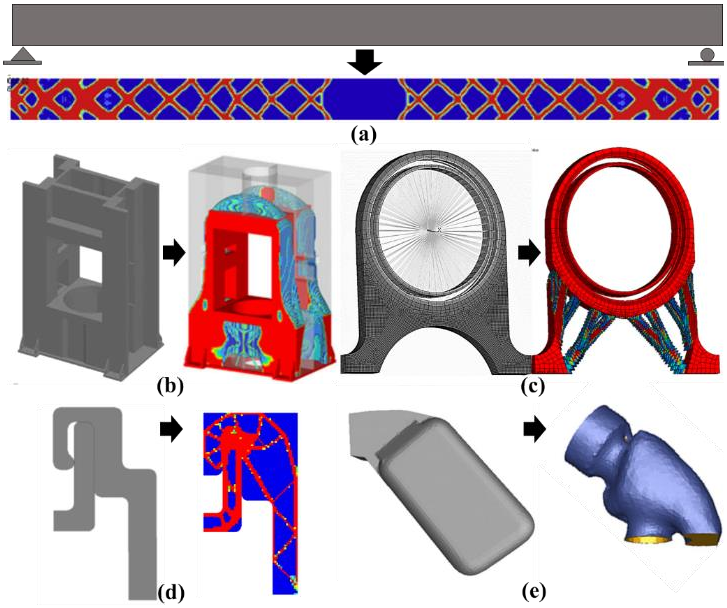

Figure 2. Topology optimization studies, (a) steel perforated beam [40], (b) fine blanking press [41], (c) roller bearing housing [38], (d) photovoltaic panel connector [42], (e) vibro-acoustic hearing instrument [39]

2. MODELING AND CALIBRATION

This section presents a detailed description for the numerical modeling of the ring-shaped steel plate shear wall using ABAQUS. The selected specimen (specimen 2-13-1) has the best performance among the proposed ring-shaped models (see Fig. 1). The yield stress and strain (σy, εy), ultimate stress and strain (σu, εu), modulus of elasticity (E), Poisson's ratio (υ) and the stress-strain curve are shown in Fig 3.

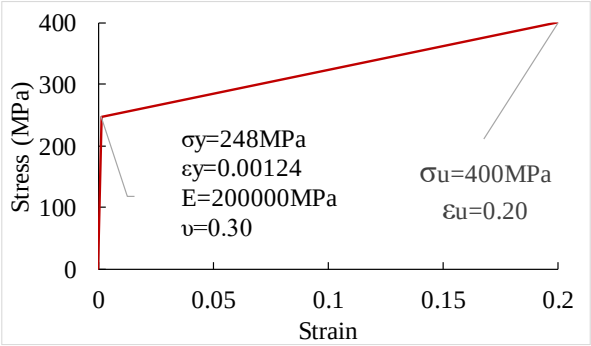

Figure 3. Stress-strain curve for finite element modeling

It is assumed all forces are transferred by the bolt connections. Accordingly, the connection of the shear plate to the perimeter frame is fully joined using the tie connection. At the pin connection, the plate is individually modeled and connected only at three points to the angle (L8×4×7/16). In the center of the web, rotation around the z-axis (Rz) and in the up and down of web rotation around the z-axis (Rz) and the transition on the x-y plane (Ux & Uy) are released. All degrees of freedom are constrained at the junction location of the holder frame to the ground (see Fig. 4). The nonlinear behavior of material and geometry is considered. The isotropic hardening rule is utilized for material properties [45, 46]. The automatic stabilization with the specified damping factor rule is used to investigate the surface wrinkling, material instability and local buckling. In the automatic stabilization method, a constant damping factor is utilized in any nonlinear quasi-static procedure based on the global equilibrium equation (Eq. (1)).

$$P - I - F_v = 0. \qquad F_v = cM^*v. \qquad v = \frac{\Delta u}{\Delta t} \tag{1}$$

where Δu and Δt are respectively the increment of displacement and time, v is the vector of nodal velocities, M^* is an artificial mass matrix calculated with unity density, c is a damping factor, F_v is viscous forces and P and I are the external and internal forces respectively.

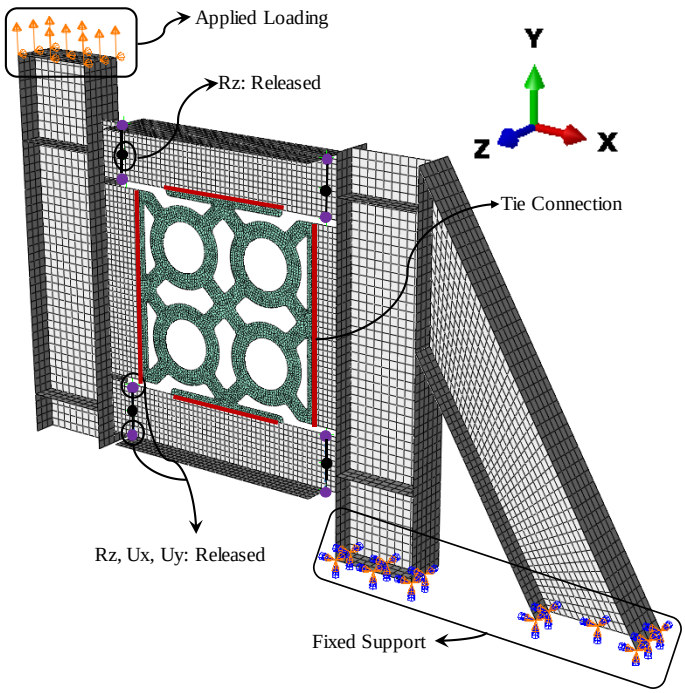

Figure 4. Finite element modeling

The loading protocol is according to ATC-24 [47]. The displacement rate is held constant throughout the loading at 25 mm/min according to the experimental condition [13], so the protocol converts to a time history loading in which the total time is equal to 7410s. The target displacements and the number of cycles for each displacement level are given in Table

1. The model is meshed using the 4-node reduced integration shell (S4R) element and analyzed through the general static module.

Table 1: Imposed displacement on the structure based on ATC 24

Level	Target displacement (mm)	Number of cycles	Drift (%)
1	2.2	3	0.25
2	3.2	3	0.37
3	4.3	3	0.5
4	8.6	3	1.0
5	13	3	1.5
6	17.3	2	2.0
7	21.6	2	2.5
8	25.9	2	3.0
9	34.5	2	4.0
10	43.2	2	5.0
11	51.8	2	6.0
12	69.1	2	8.0
13	86.4	2	10.0

Load-deformation curves of the cyclic loading for the experimental and numerical models are indicated in Fig. 5. The numerical results agree reasonably well with the experimental results reported in Egorova, Eatherton [13]. It should be noted that the shear distortion angle in Fig. 5 is based on the actual vertical displacement of the plate according to the Ref [48]. The difference between the cyclic curves is because of the perfect condition of the numerical analysis and the hardening material modeling. The deformations in the last cycle are shown and compared with the experimental model. As shown in Fig. 6, the deformations of the numerical model comply appropriately with the experimental model.

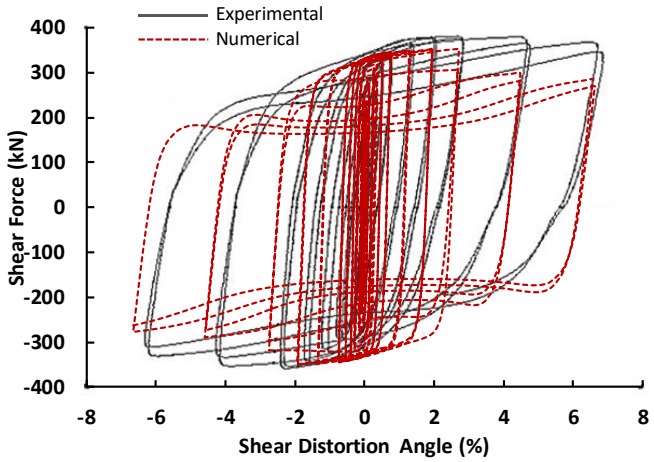

Figure 5. Force-deformation curve for numerical and experimental results

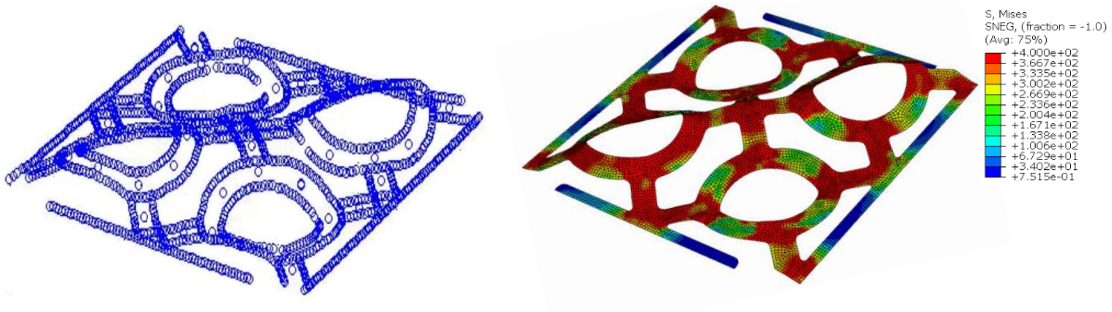

(a) Experimental deformation (b) Numerical deformation and Von Mises stress contour

Figure 6. Comparison of deformations in the last step of loading, (a) experimental model [48], (b) numerical model

3. TOPOLOGY OPTIMIZATION METHODOLOGY

In the present section, the TO procedure and parameters are described. A TO problem could be written in a general form of a problem as Eq. (2) [49]:

$$\begin{aligned} & Optimize \quad f(x) \\ Such\ that\ \ & h_j(x) = 0. \qquad j = 1.2. \ldots . n_h \\ & g_k(x) \leq 0. \qquad k = 1.2. \ldots . n_g \\ & x_l^i \leq x_i \leq x_u^i. \qquad i = 1.2. \ldots . n \end{aligned} \tag{2}$$

where f is the objective function, g_k and h_j are the inequality and quality constraint functions, n_h, n_g and n are the number of equality constraints, inequality constraints and design variables, respectively. The values x_i^l and x_i^u are the lower and upper bounds on a typical design variable x_i.

3.1 Objective function, constraints and conditions

Choosing an objective function to improve the behavior of a structure in all its aspects is very difficult. Also, the optimization based on several criteria is very complex and sometimes impossible. The main target of TO in this study is to improve the cyclic performance of the SPSW. Herein, maximization of the structural stiffness based on the strain energy is chosen as the objective function. Strain energy is the traditional and basic objective function that used to optimize the compliance and stiffness of a structure in TO [14, 50]. Based on the strain energy equation (Eq.3) and considering that the loading is imposed as a displacement pattern, the sum of strain energy of all elements must be maximized to increase the structural stiffness [43, 44].

$$\sum_{e=1}^{N} u_e^T k_e u_e = \frac{R \times D}{2} \tag{3}$$

where u_e and k_e are displacement vector and stiffness matrix of the element, respectively. R is the reaction forces and D is the imposed displacement on the structure. Based on the plate area of the ring-shaped model (314423.23mm2), the volume constraint is activated and must be less than or equal to 54% of the fill plate volume. The objective function is assigned to the whole model, but the constraint is only considered on the plate. The nonlinear analysis is done on the TO for considering the nonlinear effects of the materials, geometry and buckling. The displacement is applied to the structure in such a way that nonlinear behavior and buckling are occurred on the plate. For this purpose, the structure is initially pulled down to 10% drift and then pulled up to 10% drift.

For more appropriate comparison, the effect of connection length between the shear plate and L8×4×7/16 is considered. For this purpose, four initial plate forms are proposed for the TO procedure. As seen in Fig. 7, in the first case, the shear plate is fully connected to the angle (L8×4×7/16). In the second and third cases, the ratios of connection length to the shear plate length are respectively equal to 0.65 and 0.15. In the fourth case, the connection between shear plate and L8×4×7/16 is completely removed. It should be mentioned that the length of connection in the second and third case is based on the ring-shaped model (see Fig. 7).

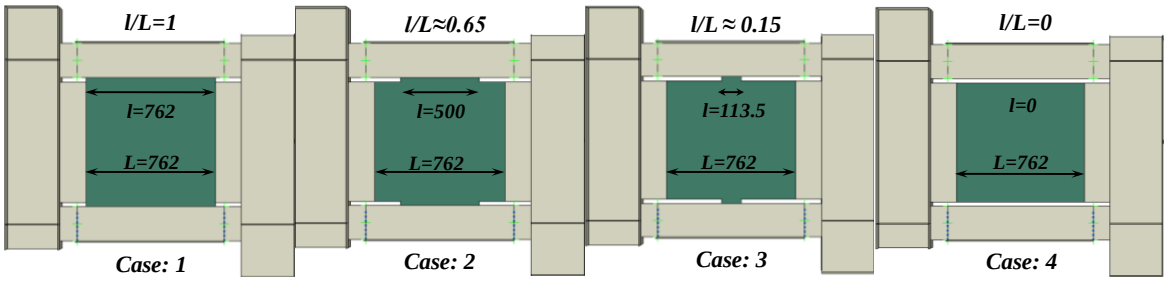

Figure 7. Initial forms of plate in TO (All dimensions are in millimeter)

3.2 SIMP method

The main purpose of TO is to eliminate the stiffness or mass of some elements with respect to the objective function and constraints. In each iteration of TO process and based on the solution method, some elements are deleted (E=0) and the other elements remained (E=1). SIMP (Simple Isotropic Material with Penalization) is one of the traditional methods to generate the relation between density and stiffness of elements. The idea of using a penalized variable density approach for numerically approximating the 0-1 design problem was studied by Bendsøe [51] and Yang & Chuang [52], and has since been used extensively. The SIMP material interpolation scheme is defined by Eq. (4):

$$E = E_0 \rho^p \tag{4}$$

where E_0 is Young's modulus of the fill or original element, E and ρ are the material stiffness and density of the unknown material, respectively, and p is the penalty exponents that must be more than 1 ($p \geq 1$). The numerical results of previous studies indicate p=3 is a suitable value [14].

3.3 Solution method

A TO problem based on the SIMP method in which the objective function (Θ) is to maximize the sum of strain energy can be written according to Eq. (5):

$$\max: \Theta = U^T K U = \sum_{e=1}^{N} (\rho_e)^p \, u_e^T \, k_e u_e$$
$$subject\ to: \begin{cases} \dfrac{V(x)}{V_o} = f \\ KU = F \\ 0 < \rho_{min} < \rho_e < 1 \end{cases} \tag{5}$$

where U and F are respectively the global displacement and force vectors, K is the global stiffness matrix, u_e and k_e are respectively the displacement vector and stiffness matrix of elements, ρ_e is the density of the elements (design variable), ρ_{min} is the vector of minimum relative densities (ρ_{min}=0.001), N is the number of elements used to discretize the design domain, p is the penalization power ($p = 3$), $V(x)$ and V_0 are respectively the material volume and design domain volume, and f is the prescribed volume fraction ($f = 0.54$).

TO can be implemented through the use of optimization solution methods and finite element method. Several methods have been proposed to solve the Eq. (5) such as homogenization method, optimality criteria method (OC), level set, the method of moving asymptotes (MMA), genetic algorithms. In this paper, the OC and MMA methods are utilized as the solution methods in TO. These methods are the basic solution methods in TO [14]. The problem solving method and types of design responses which can be used to formulate the TO procedure are the main differences between these algorithms.

3.3.1 Optimality criteria method (Condition - Based)

OC method for continuum models was studied and developed by Prager and Taylor [53], Taylor [54] and Masur [55]. The OC or condition-based algorithm is used as a suitable approach for large-scale and structural problems [14]. This algorithm uses the strain energy and stresses at the nodes as input data without calculating the local stiffness of the design variables. In the initial step, the total mass is uniformly and fully distributed in the structure. In continue, the remaining mass is redistributed in the structure based on the strain energy density and according to the volume fraction. Using this method, the area of a structure with the high density of strain energy has more mass density. In summary, the OC method uses an effective algorithm for optimization, but it is only used for structural problems. Moreover, the strain energy and volume fraction must be selected as the objective function and constraint, respectively [14, 56]. The following fix-point type update scheme (Eq. (6)) is used for the density variables [14]:

$$\rho_e^{new} = \begin{cases} \max(\rho_{min}.\rho_e - m). & if\ \rho_e B_e^{\eta} \le \max(\rho_{min}.\rho_e - m) \\ \rho_e B_e^{\eta}. & if\ \max(\rho_{min}.\rho_e - m) \le \rho_e B_e^{\eta} \le \min(1.\rho_e + m) \\ \min(1.\rho_e + m). & if\ \min(1.\rho_e - m) \le (\rho_e B_e^{\eta}) \end{cases} \tag{6}$$

where m is a positive move-limit, η is a numerical damping coefficient and B_e is determined from the optimality condition and using Lagrangian multiplier (λ) according to Eq. (7):

$$B_e = \frac{-\frac{\partial \Theta}{\partial \rho_e}}{\lambda \frac{\partial \mathrm{V}}{\partial \rho_e}} . \qquad \frac{\partial \Theta}{\partial \rho_e} = -p(\rho_e)^{p-1}\, u_e^T k_e u_e \tag{7}$$

3.3.2 Sensitivity analysis (Sensitivity-Based)

In the sensitivity-based algorithm, the density and stiffness of the design variables are simultaneously adjusted with trying to satisfy the objective function and the constraints. To obtain the optimal value, this algorithm uses the sensitivity analysis based on the design variables considering the objective function and constraints. The sensitivity analysis could be applied to all types of structural and non-structural optimization problems. In addition, the various types of objective functions such as strain energy, reaction forces, eigenvalues, etc. could be applied in this method [14, 56]. The major challenge is to apply a mathematical programming that is well geared to cope with many design variables and typically a moderate number of constraints. MMA is a mathematical programming algorithm well suited for topology design. In this method, a strictly convex approximation sub-problem is generated and solved in each step of the iteration [57]. MMA approximation uses the following scheme (Eq. (8)) to update the design variables [14]:

$$\mathrm{Optimize}\left\{\Theta(\rho^K) - \sum_{e=1}^{N}\left(\frac{(\rho_e^K - L_e)^2}{\rho_e - L_e} \times \frac{\partial \Theta}{\partial \rho_e}(\rho^K)\right)\right\} \tag{8}$$

where v_e is the volume of elements.

3.4 Stop conditions

The main stop condition of TO is the number of iterations. Furthermore, two convergence criteria are defined as the stop criterion in the TO. The first stop criterion (l_1) is the amount of changes in the objective function (Θ) from one iteration (n) to the next iteration ($n+1$). This stop criterion is defined by Eq. (9):

$$\frac{|\Theta_{\mathrm{n}+1} - \Theta_{\mathrm{n}}|}{|\Theta_{\mathrm{n}+1}|} \leq l_1 \tag{9}$$

The second stop criterion (l_2) is based on the changes in the densities (ρ) of each element from one iteration (n) to the next iteration ($n+1$) and defined by Eq. (10):

$$\frac{\sum_1^N |\rho_{n+1} - \rho_n|}{N} \leq l_2 \tag{10}$$

In this paper, the maximum number of iterations in the sensitivity and condition-based methods is respectively set to 50 and 30. In addition, at least four iterations must be conducted to terminate TO. The stop criterions l_1 and l_2 are equal to 0.001 and 0.004 respectively. When the stop criterions (l_1. l_2) achieve the determined values (0.001, 0.004), the TO is terminated without finishing the number of iterations. Note that the number of iterations is determined using trial and error on the models to obtain a clear optimized topology. The steps of TO are summarized in the flowchart of Fig. 8.

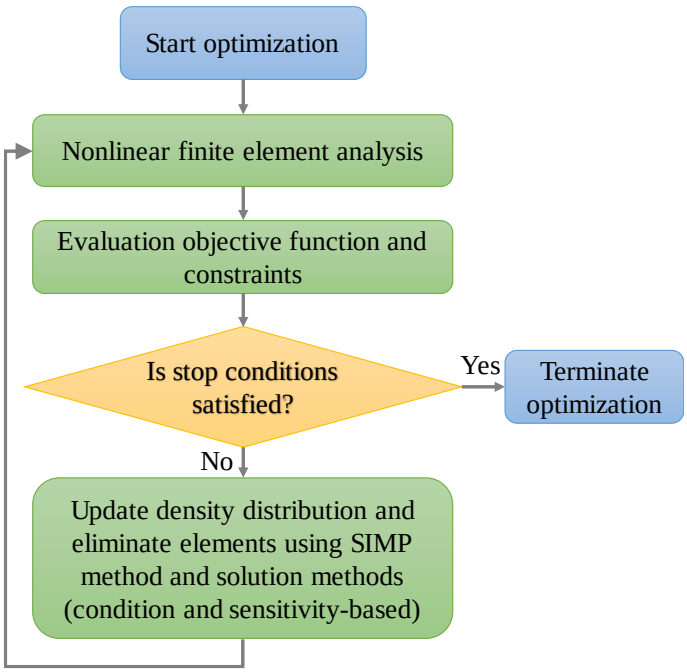

Figure 8. Topology optimization flowchart

3.5 Optimization results

By considering types of the solution method and initial plate form, eight scenarios are proposed for TO. The details of scenarios are given in Table 2. Based on the proposed scenarios, eight perforated plates are obtained. The changes of plate topology during optimization are shown in Fig. 9 and Fig. 10 for condition and sensitivity-based method, respectively. Furthermore, the values of the objective function and volume fraction during TO are shown in Fig. 11 for the condition-based and Fig. 12 for the sensitivity-based method. Considering the presented results in Figs. 9-12 the following consequences could be inferred.

Table 2: Condition of topology optimization scenarios and results (CB: Condition-Based, SB: Sensitivity-Based)

Model name	(Case No)	Solution method	Initial volume fraction	Final volume fraction	Initial objective function (kN.m)	Final objective function (kN.m)	Number of iterations
C1	1	CB	1	0.547	225.718	208.504	28
C2	2	CB	1	0.549	221.462	176.307	28
C3	3	CB	1	0.548	208.908	137.080	28
C4	4	CB	1	0.548	179.976	115.839	29
S1	1	SB	0.54	0.540	158.543	231.591	26
S2	2	SB	0.54	0.539	123.457	211.141	26
S3	3	SB	0.54	0.539	57.612	161.979	25
S4	4	SB	0.54	0.540	44.862	147.526	26

About the updating scheme of density in the condition-based method, it can be seen that in the initial iteration, the fraction density of whole elements in the plate is equal to 1. In continue, by using OC and SIMP methods (Eq. 4, 5, 6 & 7), a new value of density for each element is obtained (see Fig. 9 and Fig. 11). Based on the number of iterations, volume fraction and objective function the density of elements is reduced and the elements eliminated. As seen in Fig. 11 and Table 2, the volume fraction (constraint) is decreased about 46% during TO while the decrease of strain energy (objective function) for C1, C2, C3 and C4 is respectively equal to 7.63%, 20.4%, 34.4% and 35.6%.

In the sensitivity-based method, the density of all elements is reduced to the prescribed volume fraction (0.54) in the initial iteration. In continue, the effective elements to maximize the objective function are identified using sensitivity analysis and their densities are increased. On the other hand, the density of the other elements is reduced or eliminated. Despite the condition-based method, in the sensitivity-based method, the volume fraction is approximately constant during TO while the strain energy objective function is increased for S1, S2, S3 and S4 about 47%, 71%, 181% and 228% , respectively (See Fig. 12 and Table 2).

The number of iterations in Table 2 illustrates that stop criterions are dictated and the TO is terminated without reaching the total number of iterations. As shown in Fig. 11 and Fig. 12, the changes in the topology become very tiny by the increase of iterations. So, the stop criterions prevent from doing extra iterations with regards to time-consuming of doing nonlinear analysis in each iteration. Also, the results prove that the defined values for the stop criterions are suitable because the obtained topologies are clear and the density of all remained elements (except a few elements in the boundaries) is reached to $\rho_n = 1$. It can be seen from Fig. 11 and Fig. 12 that no slim part is created in optimization. The nonlinear analysis prevents the creation of the slim parts in the TO process because they can't increase the structural strength in nonlinear analysis.

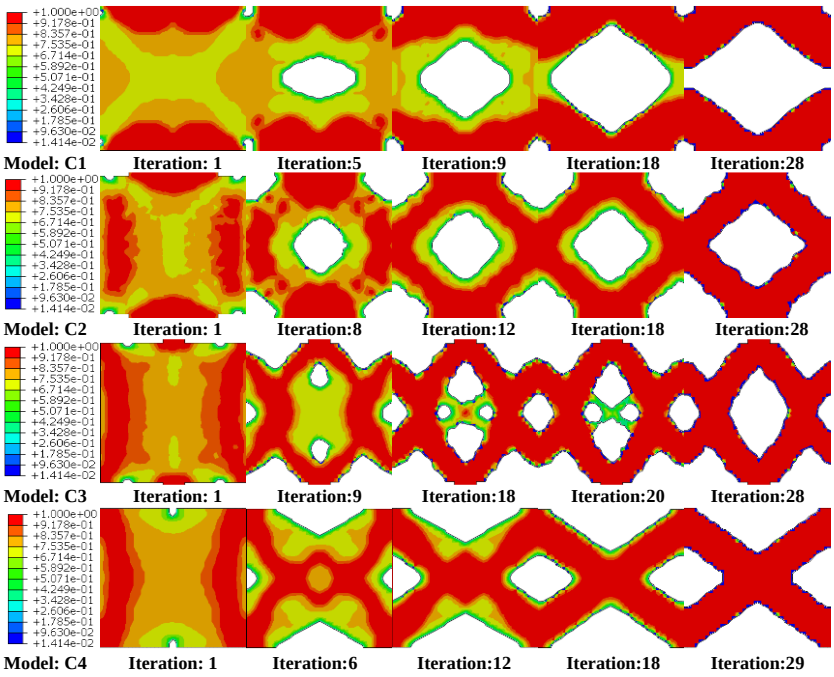

Figure 9. Changes in density contour of the plate in the condition-based method

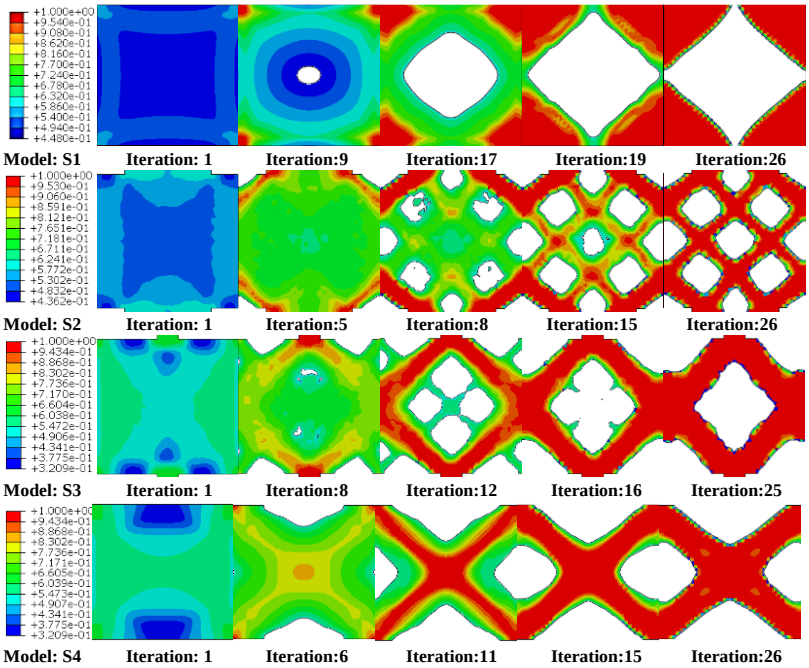

Figure 10. Changes in density contour of the plate in the sensitivity-based method

The obtained forms using TO indicate that in both solution methods, except in case 4, a hole is created in the center of the plate. The TO results prove the amount of length connection impacted on the optimized topology. The optimized form for the full connected plate has a central hole in both solution methods (C1 and S1). It illustrates that the

traditional form of the perforated plate with a central circular hole is an optimal form. The optimized form converges to the X-shaped for both solution methods, when the connection between the plate and column is completely removed (C4 and S4). The optimized forms for 0.15 connection length ratio (l/L=0.15) are generally similar for both solution methods and have a central hole (C3 and S3). But the obtained optimized form using the sensitivity-based method is completely different from the condition-based method when the connection length ratio is equal to l/L=0.65 (C2 and S2).

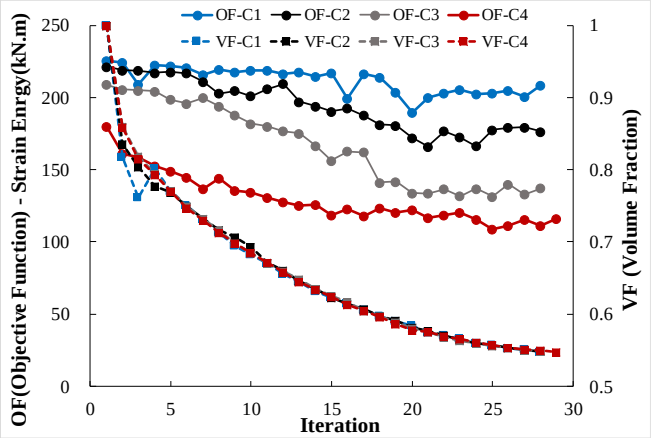

Figure 11. Objective function and volume fraction for condition-based method

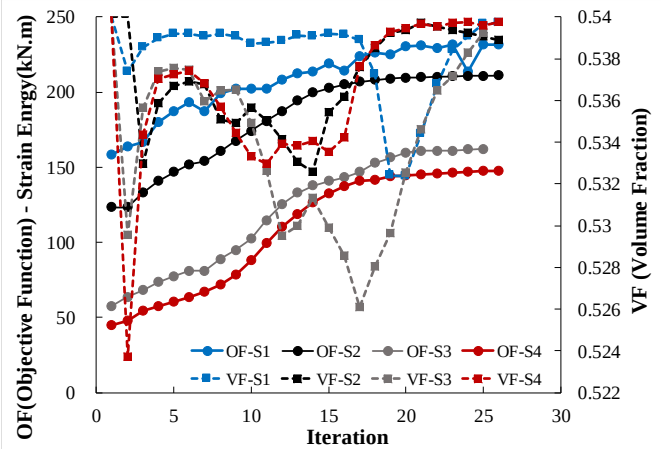

Figure 12. Objective function and volume fraction for sensitivity-based method

Finally, based on the obtained forms using TO and considering the similarity of results in case “4”, seven optimized forms are proposed (see Fig. 13). The presented dimensions are according to the TO results. As shown in Fig. 13, the area of optimized plates is approximately equal to the area of the ring-shaped plate (314423mm^2).

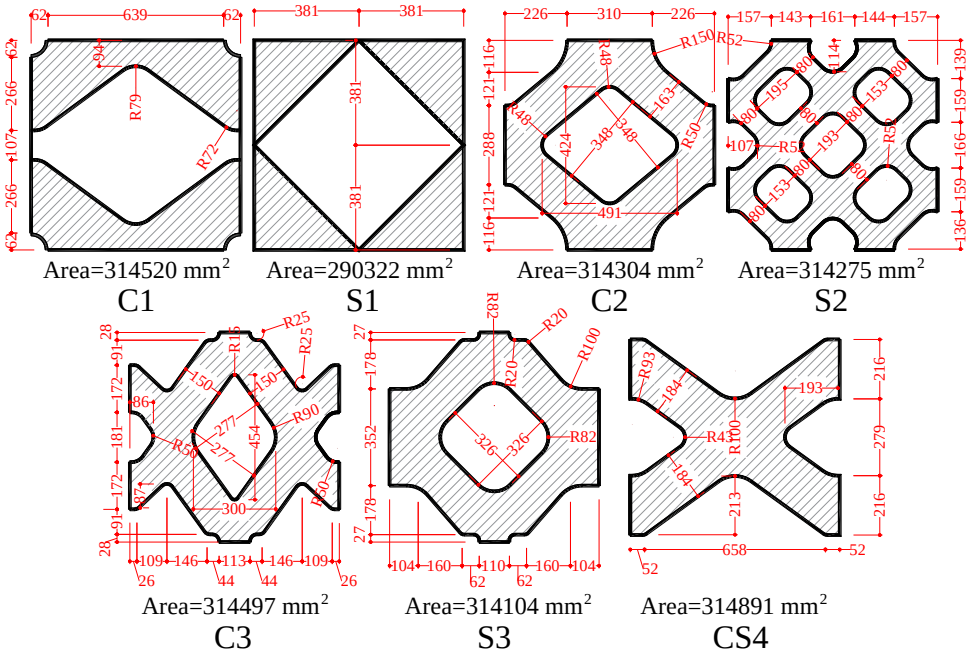

Figure 13. Proposed optimized forms (all dimensions are in millimeter)

4. NONLINEAR BEHAVIOR OF SPSWS WITH OPTIMIZED TOPOLOGY

4.1 Cyclic and monotonic behavior

In the present section, the nonlinear behavior of the optimized models is thoroughly studied. For this purpose, a nonlinear analysis is conducted under cyclic and monotonic loadings for all the optimized models. The cyclic loading is according to ATC 24 protocol that was presented in the second section. The maximum displacement in the monotonic loading is equal to 86.4mm. All the parameters and specifications of the numerical models are defined the same as the proposed numerical finite element model in the second section.

The results of nonlinear analysis due to cyclic loading are presented in Fig. 14. With comparing the cyclic curves, it can be seen that the pinching behavior occurs in all the models, but the intensity of pinching is different. Pinching behavior is related to buckling and OPD of the plate. On the other hand, the increase in strength at the end of each loop is due to the tension field action and post-buckling phenomenon. As seen in Fig. 14, in the C2 and CS4 model the initial stiffness decreases sharply due to buckling and OPD. For a better comparison, the pushes of cyclic curves are presented in Fig. 15. The results indicate the C1 and RS models have the maximum and minimum strength respectively. In addition, the stiffness is decreased after the initial cycles in all the optimized models, but the strength of the RS model is approximately constant during cyclic loading. However, because of tensile field action, the pushes of the cyclic curves for optimized models have more values than the RS model.

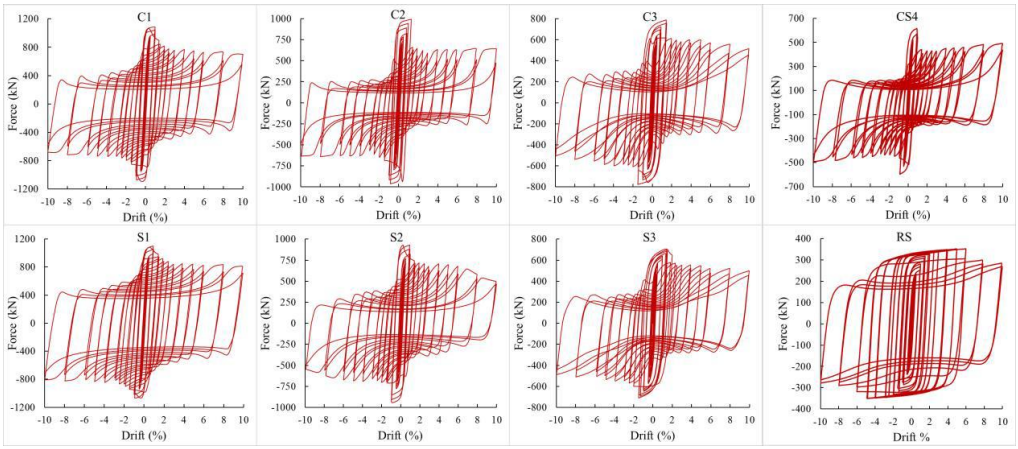

Figure 14. Force-deformation curve for cyclic loading

For a clear review, the curves of the last loop are indicated in Fig. 16. The results illustrate the S1 model has more stiffness and encloses more space than the other models. It also appears in the C1 model, but the stiffness and enclosed space by the curve are less than the S1 model. In comparison to the RS model, the C2, C3, S2, S3 and CS4 models have more strength in the tensile filed action zone, but their strengths are decreased in the pinching zone.

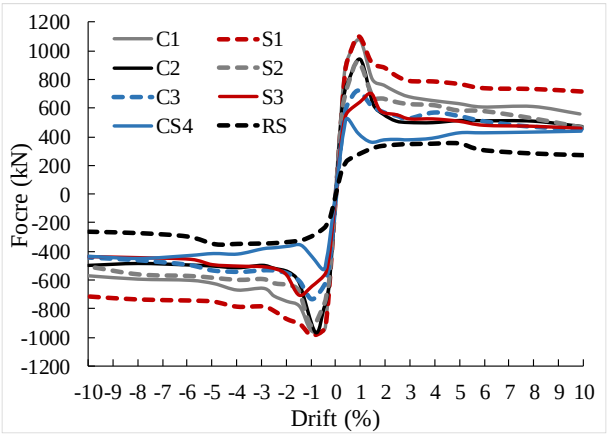

Figure 15. Push of cyclic curves

The results of monotonic loading indicate, like cyclic push curves, the C1 and RS models have the maximum and minimum values of strength respectively (see Fig. 17). For the C1 and CS4 models, strength reduction occurs in the monotonic curves at the 9.6% and 4.6% drift respectively. This reduction is due to the buckling and OPD of the plate. It can be seen from Fig. 17 that the models with similar connection length ratio have equal strength.

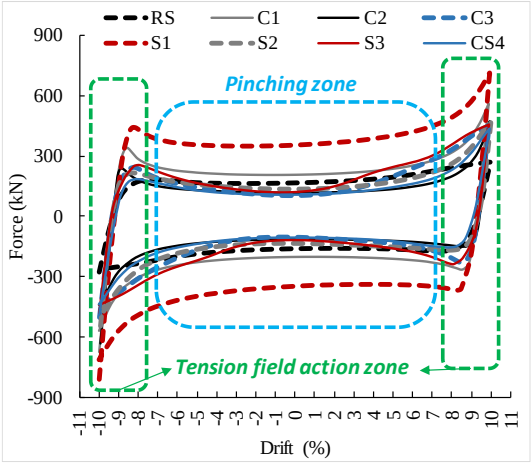

Figure 16. Force-deformation curve in the last loop

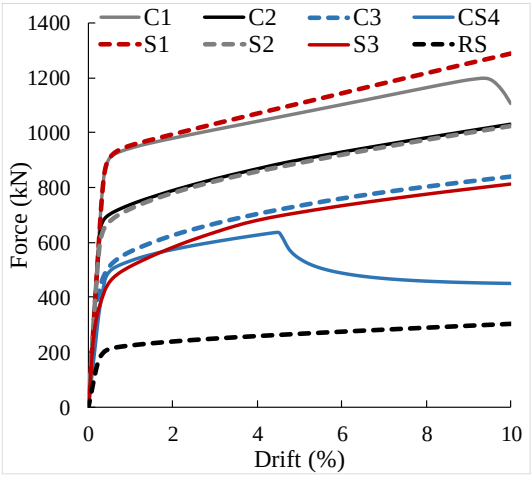

Figure 17. Force-deformation curve for monotonic loading

4.2 Stiffness and load-carrying capacity

For investigating the stiffness of the RS and optimized models, the initial (Ki) and secant stiffness (Ks) based on the monotonic loading are compared. The secant stiffness is related to the position with 2.5% inter-story drift angle (2.5% is the maximum inelastic drift according to UBC97 [58]. The method of defining the initial and secant stiffness is according to Fig. 18. Furthermore, according to the monotonic loading, the value of reaction force at yield point (Py), the maximum value of the reaction force (Pmax) and the value of reaction force at 10% drift (Pu) are measured (see Fig. 18). Also, the maximum value of reaction force in the cyclic loading (Pn) is calculated. The numerical results related to stiffness and strength of the RS and optimized models are presented in Table 3. The results indicate that the stiffness and load-carrying of all the optimized models are significantly increased. The maximum values of initial stiffness and secant stiffness belong to the C1 and S1 models respectively. The S1 model has the maximum values of Py, Pmax, Pu and Py, and the minimum values of stiffness and strength belong to the RS model.

Table 3: Values of stiffness (kN/mm) and strength (kN) for ring-shaped and optimized models

Models	Ki	Ks	Py	Pmax	Pu	Pn
RS	90	11	204	304	304	353
C1	288	46	900	1196	1105	1092
C2	284	37	692	1030	1030	992
C3	244	30	488	841	841	786
S1	280	47	912	1287	1287	1097
S2	284	37	660	1023	1023	945
S3	251	28	421	814	814	709
CS4	159	27	486	636	450	615

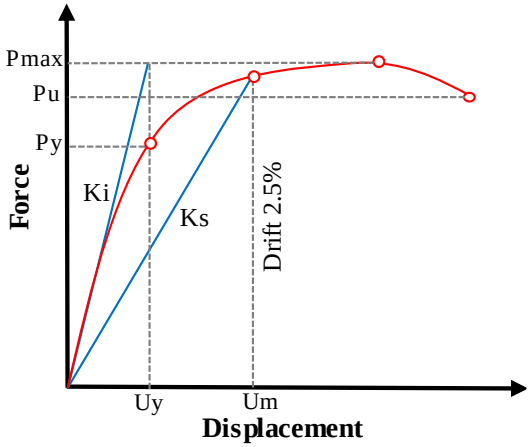

Figure 18. Initial and secant stiffness

For an appropriate comparison between the models, the ratio of stiffness and strength of the optimized models to the RS model are respectively shown in Fig. 19 and Fig. 20Figure 2. The initial stiffness for all optimized models (except CS4) is near 2.5~3 times of the RS model. The secant stiffness for C1 and S1 is near 4.0, for C2 and S2 near 3.2, for C3 and S3 near 2.5, and for CS4 near 2.4 times of the RS model. The strength of optimized models is dramatically increased. The yield and maximum strength of the optimized models are increased near 2~4 times of the RS model. Furthermore, enhancement of maximum reaction force in the cyclic loading (Pn) is near 1.7~3 times of the RS model.

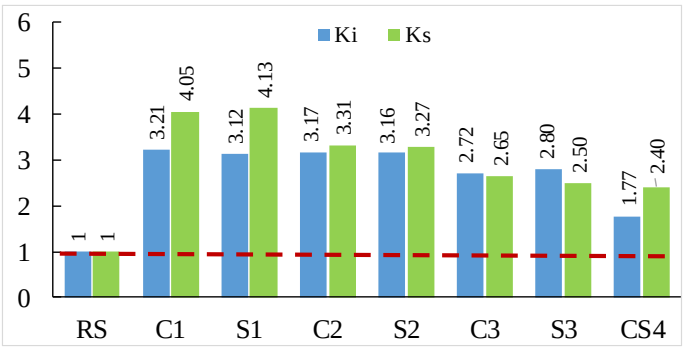

Figure 19. Ratio of stiffness of optimized models to the RS model

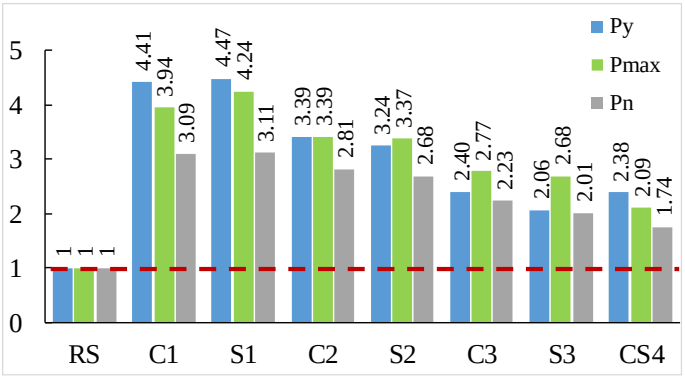

Figure 20. Ratio of strength of optimized models to the RS model

4.3 Energy dissipation and fracture tendency

The area under a load-deformation curve is equal to the energy dissipation (ED). ED of a structure is an index that includes principal components such as stiffness, strength and ductility. Fig. 21 shows ED of the RS and optimized models during the cyclic loading. By considering the Fig. 21, it can be seen that the difference between ED curves is observed after cycle 10. The S1 model has the best performance in ED, and the C1 and S2 models are respectively in the next ranks. The ED of C2 and C3 is similar and ED curve of S3 model is located at the top of C2 and C3 curve with a slight difference. Despite the increase of ED from the cycle 10 to 26 for the C2 and C3 models compared to the RS model, the curves of three models (C2, C3 and RS) after cycle 27 are very close to each other. The CS4 model has the weakest performance in the ED. The values of ED at the end of cyclic loading are presented in Table 4.

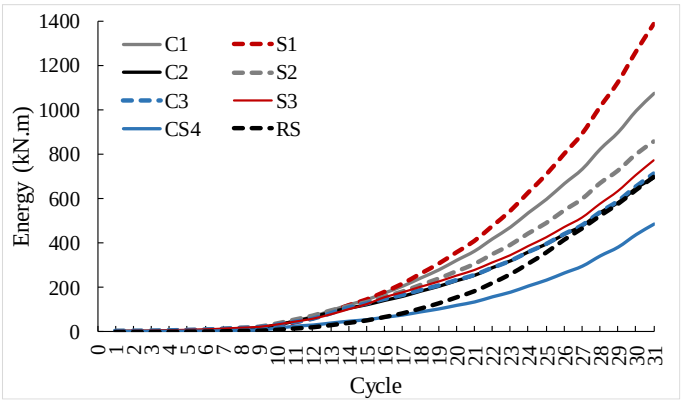

Figure 21. Energy dissipation during cyclic loading

Investigating the fracture tendency in the RS and optimized models is very important in order to judge their cyclic performance. An increase in the stiffness and energy dissipation of a structure is useful if it does not enhance the structural fracture tendency. The fracture tendency can be predicted by the equivalent plastic strain (PEEQ) defined by Eq. (11). PEEQ is described as a cumulative variable and a monotonically incremental function. This index represents the local ductility and fracture tendency of steel [44].

$$PEEQ = \dot{\varepsilon}^{pl}|_0 + \int_0^t \dot{\varepsilon}^{pl}\, dt\,.\ \dot{\varepsilon}^{pl} = \sqrt{\frac{2}{3}\dot{\varepsilon}^{pl} : \dot{\varepsilon}^{pl}} \tag{11}$$

where $\dot{\varepsilon}^{pl}$ is the rate of plastic flow, $\dot{\bar{\varepsilon}}^{pl}$ is the equivalent plastic strain rate and $\dot{\bar{\varepsilon}}^{pl}|_0$ is the initial equivalent plastic strain rate. The values of PEEQ in at the end of cyclic loading are represented in Table 4.

Table 4: Values of ED, PEEQ and OPD in the last cycle

Models	ED (kN.m)	PEEQ	OPD (mm)
RS	696.05	29.16	72.00
C1	1071.39	17.60	121.60
C2	696.21	16.20	131.00
C3	711.96	17.65	136.50
S1	1386.05	25.13	111.90
S2	858.25	6.10	113.70
S3	769.36	13.63	133.70
CS4	485.63	6.43	130.50

The results in Table 4 illustrate that the minimum and maximum values of PEEQ belong to the S2 (PEEQ=6.1) and RS (PEEQ= 29.16) models respectively. S1 model has the maximum value (25.13) of PEEQ between the optimized models. The position and distribution of PEEQ in the models are shown in Fig. 22 (red circle). By considering Table 4 and Fig. 22, it can be seen that the main reason for the high amount of PEEQ in the RS model is the stress concentration at the corner of the ring part. In the optimized models, the stresses in the plate are more appropriately distributed so the values of PEEQ are reduced. As shown in Fig. 22, the S2 model has the highest stress distribution in the plate and consequently the PEEQ value is decreased. The difference between S2 and the other models is considerable in the PEEQ. The reason for this decrease relates to the topology of the plate in the S2. The obtained form in the S2 could create various patches for stress distribution and then plastic strains are distributed with less intensity.

The maximum values of OPD of the models are shown in Table 4. The results show RS and C3 models have the lowest and highest values of OPD. The position of OPD is shown in Fig. 23 with a red circle (dashed line). Increasing the values of OPD in the optimized models often causes the exacerbation of pinching behavior. On the other hand, the results indicate that this increase reduces the fracture tendency. In fact, the OPD dissipates the stresses through post-buckling phenomenon and improves the tension field action in the plate.

For a desirable comparison between the RS and optimized models, the ratios of ED, PEEQ and OPD of the optimized models to the RS model are presented in Fig. 23. It can be seen from Fig. 23 that in comparison to the RS model, the values of ED are increased about 54% for C1, 99% for S1, 23% for S2 and 11% for S3 models. The ED values in the C2 and C3 models are not improved and even decreased about 30% in the CS4 model. The values of PEEQ with respect to the RS model are reduced near 40% for C1, C2 and C3 models, 14% for S1, 53% for S3 and 80% for S2 and CS4 models. The OPD values of all the optimized models are increased. The highest and lowest enhancements belong to C3 and S1 models, respectively that are equal to 1.90 and 1.55 times of the RS model.

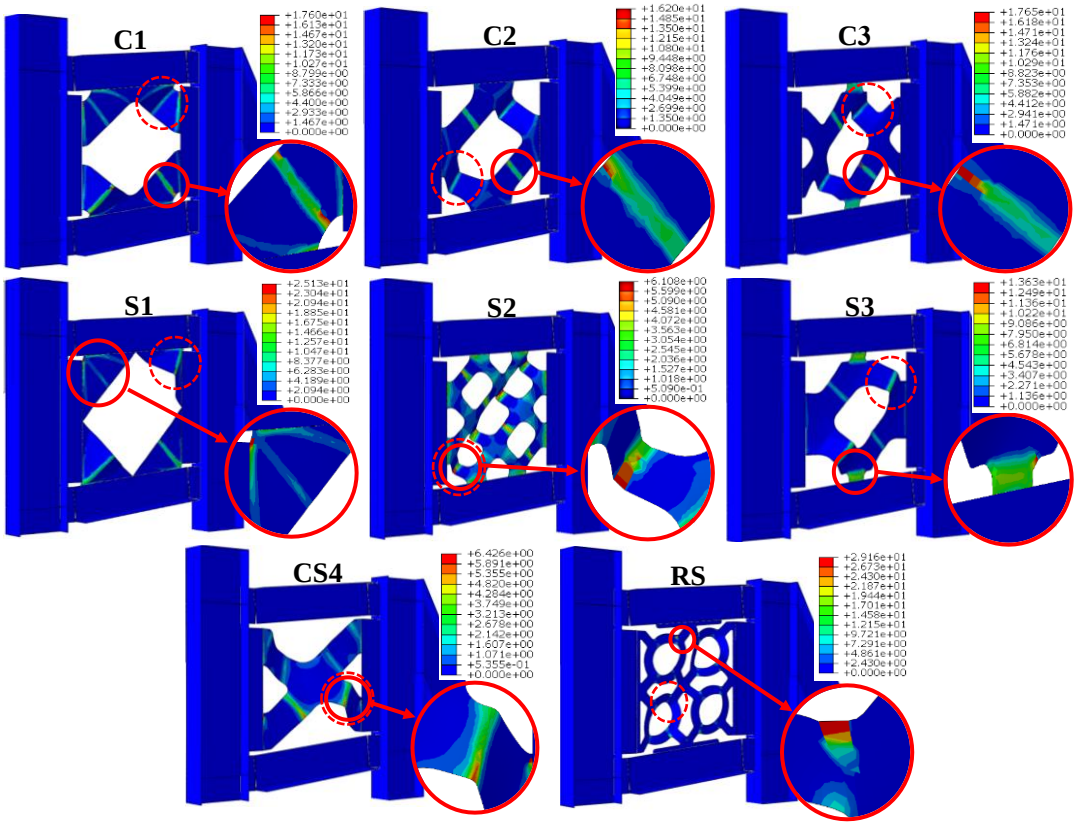

Figure 22. PEEQ contour at the end of cyclic loading, max PEEQ (red circle) and max OPD (dashed red circle)

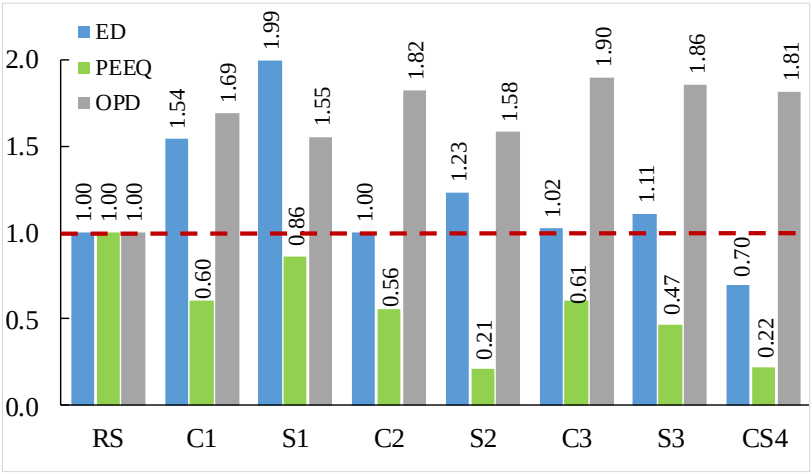

Figure 23. Ratio of energy dissipation, equivalent plastic strain, and out-of-plane deformation of optimized models to the ring-shaped model

5. ACCEPTABLE AND UNACCEPTABLE FORMS

Herein, a brief description and clear decision are presented about the optimized forms based on the obtained results in the fourth section.

- S1 model (acceptable): no significant strength reduction is observed in the cyclic loading. The push of load-deformation in the cyclic loading is the best. It is the best with significant difference in the pinching zone. No strength reduction in the monotonic loading is observed. It is the best in the energy dissipation. In this model, the fracture tendency is maximum between the optimized models but less than the RS model.
- S2 model (acceptable): in comparison with the RS and optimized models, the fracture tendency is decreased significantly (near 80%). The strength and stiffness are increased near 3 times of the ring-shaped model. Also, ED is enhanced about 23% in comparison to the ring-shaped model. This model has suitable performance in both the increase of strength and decrease of fracture tendency.
- S3 model (unacceptable): the PEEQ has reduced about 53% in comparison with RS model. In the energy dissipation, it is located in the fourth rank and better than the RS model (11% at the end of cyclic loading). The pinching behavior is near to the S2 model. Compared to model S2, the choice is not logical.
- C1 model (unacceptable): a significant strength degradation is observed in the monotonic loading. Despite a tiny difference in geometry comparing with S1, a considerable reduction occurred in the strength, pinching behavior and energy dissipation.
- C2 model (unacceptable): after primary structural stiffness, the push of cyclic loadings is less than the S2 model. Energy dissipation, fracture tendency and pinching behavior are weak in comparison to S2. Compared to model S2, the choice is not reasonable.
- C3 model (unacceptable): in comparison with the other optimized models it is located in the sixth rank and the choice is not reasonable.

CS4 model: (unacceptable): the push of cyclic loading is near to the RS model. Energy dissipation is less than RS. A significant strength degradation is observed in the monotonic loading.

6. CONCLUSION

In this paper, the effect of connection length between column and shear plate was investigated in the TO results. Also, the effect of two basic solution methods in the results of optimization was considered. The main findings in the TO process and results briefly include the followings:

1. The changes in the connection length between the shear plate and column were significantly impacted on the TO results.
2. The TO results with the use of sensitivity and condition based method for l/L=0 were completely similar, for l/L = 1 and l/L =0.15 had a partially different and for l/L=0.65 were completely different.
3. The TO results proved that a plate with a central circular hole (the traditional form of a perforated plate) could be an optimal form for the shear plate with l/L =1.

4. Doing nonlinear analysis in each iteration of TO prevented from creating slim parts in the optimized plate.

All optimized models were analyzed under cyclic and monotonic loadings and the results compared with the RS model. The results indicated that a small change in the holes could cause a major change in the structural behavior. For example, although there was a very tiny difference between obtained topology for S1 and C1, the results showed the behavior of S1 in cyclic and monotonic loadings, pinching behavior and energy dissipation is better than the C1 despite the area of the plate in S1 model being less than C1. To summarize the investigation of the analysis, the results are briefly discussed in six topics:

1. Stiffness and load-carrying: The stiffness and load-carrying capacity of all the optimized models have significantly improved compared with the RS model. S1 and CS4 models had the maximum and minimum values of stiffness and strength respectively between the optimized models.
2. Energy dissipation: The energy dissipation of S1, C1, S2 and S3 models has respectively increased near 99%, 54%, 23% and 11% compared with the RS model. There was no improvement for C2 and C3 models, and even a reduction near 30% was observed in the CS4 model.
3. Fracture tendency: The fracture tendency was predicted using the equivalent plastic strain (PEEQ). The values of PEEQ for all optimized models have reduced in comparison with the RS model. It was observed that the stress distribution and consequently PEEQ distribution in the optimized models were more appropriate than the RS model. The values of PEEQ in S1 and S2 models were equal to 86% and 21% of the RS model respectively.
4. Pinching behavior: The buckling and out-of-plane deformation (OPD) are two effective parameters in the pinching behavior. In the optimized models, S1and C1 had the best pinching behavior. In the other optimized models, no improvement in the pinching behavior was observed in comparing with the RS model. The values of OPD in all optimized models were more than the RS model. Although decreasing of OPD in the RS model improved the pinching behavior, but increasing OPD and buckling caused an improvement in the tension field action and PEEQ.
5. Connection length ratio: The results illustrated the stiffness and fracture tendency were increased with the increase of connection length ratio (l/L). In an overall view and based on the results, a balance between the stiffness and fracture tendency was observed for the connection length ratio l/L=0.65.
6. TO solution methods: The nonlinear behavior of the optimized plate indicated the obtained optimized plates by the sensitivity-based method (especially S1 and S2 models) had better performance in comparison with the condition-based method.

Based on the presented results, the S1 and S2 models are two acceptable forms as a perforated steel plate shear wall. In the S1 model, the stiffness, strength and energy dissipation dramatically increased. In this model, the pinching behavior was completely suitable, and the fracture tendency reduced near 14% compared with the RS model. In the S2 model, the stiffness and strength increased by about 300%, the energy dissipation increased about 23% while the value of PEEQ reduced about 80% compared with the RS model. This model presented a balanced behavior for both stiffness and fracture tendency.

REFERENCES

1. Roberts TM, Ghomi SS. Hysteretic characteristics of unstiffened plate shear panels, *Thin Walled Struct* 1998; **12**(2): 145-62.
2. Berman JW, Bruneau M. Experimental investigation of light-gauge steel plate shear walls, *J Struct Eng* 2005; **131**(2): 259-67.
3. Emami F, Mofid M, Vafai A. Experimental study on cyclic behavior of trapezoidally corrugated steel shear walls, *Eng Struct* 2013; **48**: 750-62.
4. Farzampour A, Laman JA. Behavior prediction of corrugated steel plate shear walls with openings. *J. Constr. Steel Res.* 2015; **114**: 258-268.
5. Jin S, Ou J, Liew JYR. Stability of buckling-restrained steel plate shear walls with inclined-slots: theoretical analysis and design recommendations, *J Constr Steel Res* 2016; **117**: 13-23.
6. Ghomi SS, Kharrazi MHK, Azizi SM, Sajadi RA. Buckling behavior improvement of steel plate shear wall systems, *Struct Des Tall Spec Build* 2008; **17**(4): 823-37.
7. Alavi E, Nateghi F. Experimental study of diagonally stiffened steel plate shear walls, *J Constr Steel Res* 2013; **139**(11): 1795-81.
8. Akbari A, Mofid H, Mofid M. On the experimental and numerical study of braced steel shear panels, *Struct Des Tall Spec Build* 2015; **24**(14): 853-72.
9. Robert TM, Ghomi SS. Hysteretic characteristics of unstiffened perforated steel plate shear panels, *Thin-Walled Struct* 1992; **14**(2): 139-51.
10. Hitaka T, Matsui C. Experimental study on steel shear wall with slits, *J Struct Eng* 2003; **129**(5): 586-95.
11. Chen SJ, Jhang C. Experimental study of low-yield-point steel plate shear wall under in - plane load, *J Constr Steel Res* 2011; **97**(6): 977-85.
12. Wang M, Yang W, Shi Y, Xu J. Seismic behaviors of steel plate shear wall structures with construction details and materials, *J Constr Steel Res* 2015; **107**: 194-210.
13. Egorova N, Eatherton MR, Maurya A. Experimental study of ring-shaped steel plate shear walls, *J Constr Steel Res* 2014; **103**: 179-89.
14. Bendsøe M, Sigmund O. *Topology Optimization: Theory, Methods, and Applications*, 2nd ed, Springer-Verlag Berlin Heidelberg, New York, NY, USA, 2003.
15. Bendsøe MP, Kikuchi N. Generating optimal topologies in structural design using a homogenization method, *Comput Meth Appl Mech Eng* 1988; **71**(2): 197-224.
16. Maute K, Schwarz S, Ramm E. Adaptive topology optimization of elastoplastic structures, *Struct Optim* 1998; **15**(2): 81-91.
17. Buhl T, Pedersen CBW, Sigmund O. Stiffness design of geometrically nonlinear structures using topology optimization, *Struct Multidiscip Optim* 2000; **19**(2): 93-104.
18. Ansola R, Canales J, Tarrago JA, Rasmussen J. An integrated approach for shape and topology optimization of shell structures, *Comput Struct* 2002; **50**(5): 449-548.
19. Ye HL, Wang WW, Chen N, Sui YK. Plate/shell topological optimization subjected to linear buckling constraints by adopting composite exponential filtering function, *Acta Mech Sin* 2016; **32**(4): 649-58.
20. Liu A, X.Huang, C.Huang, G S, Yan X, Li G. Topological design of structures under dynamic periodic loads, *Eng Struct* 2017; **142**: 128-36.

21. Khatibinia M, Naseralavi SS. Truss optimization on shape and sizing with frequency constraints based on orthogonal multi-gravitational search algorithm, *J Sound Vib* 2014; **333**(24): 6349-69.
22. Kaveh A, Mahdavi V.R. Colliding bodies optimization for size and topology optimization of truss structures, *Struct Eng Mech* 2015; **53**(5): 847-65.
23. Khatibinia M, Yazdani H. Accelerated multi-gravitational search algorithm for size optimization of truss structures, *Swarm Evol Comput* 2018; **38**: 109-19.
24. Seyedpoor S, Gholizadeh S. Optimum shape design of arch dams by a combination of simultaneous perturbation stochastic approximation and genetic algorithm methods, *Adv Struct Eng* 2008; **11**(5): 501-10.
25. Khatibinia M, Khosravi S. A hybrid approach based on an improved gravitational search algorithm and orthogonal crossover for optimal shape design of concrete gravity dams, *Appl Soft Comput* 2014; **16**: 223-33.
26. Mahani AS, Shojaee S, Salajegheh E, Khatibinia M. Hybridizing two-stage meta-heuristic optimization model with weighted least squares support vector machine for optimal shape of double-arch dams, *Appl Soft Comput* 2015; **27**: 205-18.
27. Gholizadeh S, Barati H. Topology optimization of nonlinear single layer domes by a new metaheuristic, *Steel Compos Struct* 2014; **16**(6): 681-701.
28. Kaveh A, Rezaei M. Topology and geometry optimization of single-layer domes utilizing CBO and ECBO, *Sci Iran Transaction A, Civil Eng* 2016; **23**(2): 535.
29. Kaveh A, Rezaei M. Topology and geometry optimization of different types of domes using ECBO, *Adv Comput Des* 2016; **1**(1): 1-25.
30. Sousa LC, Castro CF, António CC, Sousa H. Topology optimisation of masonry units from the thermal point of view using a genetic algorithm, *Constr Build Mater* 2011; **25**(5): 2254-62.
31. Das R, Jones R, Xie YM. Optimal topology design of industrial structures using an evolutionary algorithm, *Optim Eng* 2011; **12**(4): 681-717.
32. Lee EH, Park J. Structural design using topology and shape optimization, *Struct Eng Mech* 2011; **38**(4): 517-27.
33. Stromberg LL, Beghini A, Baker WF, Paulino GH. Topology optimization for braced frames: Combining continuum and beam/column elements, *Eng Struct* 2012; **37**: 106-24.
34. Kutyłowski R, Rasiak B. Application of topology optimization to bridge girder design, *Struct Eng Mech* 2014; **51**(1): 39-66.
35. Gao X, Ma H. Topology optimization of continuum structures under buckling constraints, *Comput Struct* 2015; **157**: 142-52.
36. Allahdadian S, Boroomand B. Topology optimization of planar frames under seismic loads induced by actual and artificial earthquake records, *Eng Struct* 2016; **115**: 140-54.
37. Dang H, Lee D, Lee K. Single and multi-material topology optimization of CFRP composites to retrofit beam-column connection, *Comput Concr* 2017; **19**(4): 405-11.
38. Kabus S, Pedersen CBW. Optimal bearing housing designing using topology optimization, *J Tribol* 2012; **134**(2): 1-9.
39. Søndergaard MB, Pedersen CBW. Applied topology optimization of vibro-acoustic hearing instrument models, *J Sound Vib* 2014; **333**(3): 683-92.
40. Tsavdaridis KD, Kingman JJ, Toropov VV. Application of structural topology optimisation to perforated steel beams, *Comput Struct* 2015; **158**: 108-23.

41. Zhao X, Liu Y, Hua L, Mao H. Finite element analysis and topology optimization of a 12000KN fine blanking press frame, *Struct Multidiscip Optim* 2016; **54**(2): 375-89.
42. Lu X, Xu J, Zhang H, Wei P. Topology optimization of the photovoltaic panel connector in high-rise buildings, *Struct Eng Mech* 2017; **62**(4): 465-75.
43. TOSCA. V.8.0, Tosca Structure Documentation, Dassault Systèmes Company, Karlsruhe, Baden-Württemberg, Germany, 2013.
44. ABAQUS. V.6-14, Analysis User's Manual, Dassault Systèmes Simulia, Providence, RI, USA, 2014.
45. Maurya A. Computational simulation and analytical development of buckling resistant steel plate shear wall (br-spsw), M.S. Thesis. Virginia Polytechnic Institute and State University Department of Civil and Environmental Engineering, 2012.
46. Maurya A, Egorova N, Eatherton MR. Development of ring-shaped steel plate shear walls, *Proceedings of the 2013 ASCE Structures Congress*, Pittsburgh, 2013.
47. ATC-24, Guidelines for cyclic seismic testing of components of steel structures for buildings, Applied Technology Council, Redwood City, California, USA, 1992.
48. Egorova N. Experimental study of ring-shaped steel plate shear walls, M.S. Thesis. Virginia Polytechnic Institute and State University, Department of Civil and Environmental Engineering, 2013.
49. Hassani B, Hinton E. *Homogenization and Structural Topology Optimization*, Springer - Verlag, London, UK, 1999.
50. Lee E. A strain based topology optimization method. Ph.D. Thesis, Rutgers, The State University of New Jersey, Graduate School-New Brunswick, 2011.
51. Bendsøe MP. Optimal shape design as a material distribution problem, *Struct Optim* 1989; **1**(4): 193-202.
52. Yang RJ, Chuang CH. Optimal topology design using linear programming, *Comput Struct* 1994; **52**(2): 265-76.
53. Prager W, Taylor JE. Problems of optimal structural design, *J Appl Mech* 1968; **35**(1): 102-6.
54. Taylor JE. Maximum strength elastic structural design, *J Eng Mech Div* 1969; **95**(3): 653-63.
55. Masur EF. Optimum stiffness and strength of elastic structures, *J Eng Mech Div* 1970; **96**(5): 621-40.
56. Bakhtiary N, Allinger P, Friedrich M, Mulfinger F, Sauter J, Müller O, Puchinger M. A new approach for sizing, shape and topology optimization, *SAE International Congress and Exposition Detroit*, Michigan USA, 1996.
57. Svanberg K. The method of moving asymptotes - A new method for structural optimization, *Int J Numer Meth Eng* 1987; **24**(2): 359-73.
58. UBC97, Structural Engineering Design Provision, Uniform Building Code, USA; 1997.